nature reviews physics

https://doi.org/10.1038/s42254-026-00977-y

Review article

Check for updates

Microscale droplets for mechanical measurement and mechanotransduction in artificial and living systems

Yuyan Su[1,6], Nicholas Su[2,6], Sangwoo Kim[3] ✉, Alexandre Persat[4] ✉, Hagan Bayley[2,5] ✉ & Yujia Zhang[1] ✉

Abstract

Despite advances in the investigation of nanoscopic mechanobiology and the development of macroscale mechanotransduction, methods capable of operating at the microscale remain limited. This Review describes the physical principles and engineering of microscale droplets, including liquid constructs and hydrated polymer (hydrogel) beads, which are emerging as versatile biointerfaces for mechanical measurement and mechanotransduction in living matter. The microscale compositions and mechanical properties of droplets recapitulate key aspects of cellular mechanical responses, enabling non-invasive mechanical detection. Furthermore, droplets can contain stimulus-responsive materials that enable the transduction of mechanical cues into diverse biochemical or bioelectrical outputs. Applications of microscale droplets include cellular force and viscoelasticity sensors deployed in intercellular or intracellular environments, as well as synthetic carriers for controlled drug release and the modulation of biological activities.

Sections

[1]Laboratory for Bio-Iontronics (BION), Institute of Electrical and Micro Engineering, École Polytechnique Fédérale de Lausanne (EPFL), Lausanne, Switzerland. [2]Department of Chemistry, University of Oxford, Oxford, UK. [3]Institute of Mechanical Engineering, École Polytechnique Fédérale de Lausanne (EPFL), Lausanne, Switzerland. [4]Global Health Institute, École Polytechnique Fédérale de Lausanne (EPFL), Lausanne, Switzerland. [5]Institute of Materials and Devices for Life Sciences, Ellison Institute of Technology, Oxford, UK. [6]These authors contributed equally: Yuyan Su, Nicholas Su. ✉e-mail: sangwoo.kim@epfl.ch; alexandre.persat@epfl.ch; hagan.bayley@chem.ox.ac.uk; yujia.zhang@epfl.ch

Key points

- Microscale droplets provide cell-sized interfaces for measuring and transducing mechanical cues in biological and synthetic systems.
- Droplet mechanosensing and mechanotransduction are enabled by biophysical mechanisms such as changes in droplet morphology, membrane-channel gating, membrane flexoelectricity and deformation-dependent capacitance.
- Droplets can serve as both passive sensors and active probes for the measurement of biomechanical properties.
- Droplets can convert mechanical cues into biochemical outputs.
- Droplet networks offer a route towards multicompartment systems that couple mechanical sensing, signal transmission and actuation.

Introduction

Mechanical forces are integral to biological systems and can actively regulate cell behaviour. Examples include shear stress from fluid flow in vascular systems, which maintains vascular homeostasis[1,2]; tensile stress that mediates tactile sensation[3]; and osmotic pressure that regulates bacterial physiology[4,5]. These phenomena are mediated by two interlinked processes[6]: mechanosensation, by which cells detect mechanical stimuli, and mechanotransduction, by which these stimuli are converted into biological responses.

Various artificial systems, analogous to biological systems, have been developed to achieve mechanosensation and mechanotransduction. At the nanoscale, examples include DNA-functionalized artificial mechanoreceptors that can sense tensile force on cell membranes[7] or transduce input forces into output signalling for tissue patterning[8]. At the macroscale, advances include iontronic skin mimics[9–11]; piezoelectric, piezoresistive and triboelectric materials for wearable mechanosensors[12–14]; and ultrasound-based systems for localized mechanical stimulation for cancer[15] and osteoarthritis[16] therapies.

Bridging the gap between these nanoscale and macroscale approaches, artificial microscale droplets offer a unique, versatile platform for investigating mechanics and mechanotransduction at a biologically relevant mesoscopic scale. Broadly defined, droplets are small volumes of liquid or gel, including coacervates[17,18], liposomes[19], vesicles[20], polymersomes[21], proteinosomes[22], colloidosomes[23], water–oil emulsions[24,25], and colloidal and granular gels[26]. Unlike nanoscale molecular probes that report highly localized molecular forces or membrane events[27,28], microscale droplets respond to and transduce mechanical signals over a cell-sized volume. Their miniature size has enabled droplets to be injected into cells (femtolitre–picolitre in volume, a few micrometres in diameter)[29] or interstitial spaces (picolitre–nanolitre in volume, tens of micrometres in diameter)[30,31], which allows the investigation and modulation of cellular behaviour from a proximal location at the cellular scale[32]. Such cues are challenging to deliver internally by conventional external macroscale matrices, which function at the tissue scale and cannot therefore access subcellular environments and impose localized biochemical and mechanical effects.

In addition to their unique spatial attributes, microscale droplets possess several distinctive features that favour mechanical measurements and mechanotransduction. First, the surface and interfacial properties of droplets, including flexoelectricity and tension-dependent changes in membrane capacitance, provide well-defined mechanosensing mechanisms that convert mechanical deformation into electrical or chemical signals. Second, droplets can incorporate diverse sensing and transduction materials in a miniaturized and confined manner. Furthermore, the responses of droplet-based systems bridge a broad range of timescales. They can capture membrane events, such as ion-channel gating[33], on the millisecond timescale; probe tissue mechanics at up to approximately 1 hour with magnetically actuated ferrofluid droplets[34,35]; and report residual elasticity over days to weeks by using hydrogel-based droplets[36]. However, droplet platforms have not been developed to span the full temporal range, which is constrained by a trade-off between material stability, actuation strength and readout sensitivity. Nonetheless, in many cases, droplets can act as devices at biointerfaces that detect specific mechanobiological events (Table 1) and convert these signals into downstream biochemical or electrical outputs.

Multiple droplets can be assembled into droplet networks with the support of droplet interface bilayers (DIBs)[37–39]. In these assemblies, DIBs stabilize droplet–droplet contacts while preserving compartmentalization, thereby enabling the formation of spatially defined architectures at high resolution[40–43]. Such bilayer interfaces are also well suited to support membrane-based electrical phenomena, including capacitance changes and flexoelectric coupling, thereby creating opportunities for mechanoelectrical signal transduction in multicompartment systems[44]. Beyond isolated droplets that primarily report local responses, DIB-based droplet networks may offer a useful framework for probing how mechanical perturbations are distributed across neighbouring compartments, opening opportunities to study intercellular mechanical communication in tissues. Droplet networks can also be patterned with defined geometries to reproduce tissue-like architectures[38,39] and impose spatially organized mechanical gradients. This creates opportunities to investigate how such gradients regulate development, as well as to actively impose instructive mechanical cues to guide embryonic patterning and organoid morphogenesis[45,46]. In addition, such networks may support closed-loop coupling between sensing and actuation.

In this Review, we provide an overview of the biophysical mechanisms of droplet-enabled mechanical measurement and mechanotransduction, focusing on surface morphology, mechanosensitive membrane channels, flexoelectricity and capacitive signalling. We adopt a broad definition of 'droplet' (Box 1) to provide a comprehensive framework for discussion. We focus on the use of mechanoresponsive droplets as in situ biomechanical probes and droplet-based mechanotransduction for biotechnology. We also discuss examples involving synthetic cells and protocells, which provide mechanistic insights and design principles relevant to mechanotransduction in living systems and serve as model systems for future biological applications. Finally, we discuss the challenges and future directions in this emerging field, envisioning droplet systems as components of next-generation biointerfaces for decoding and programming the mechanics of life.

Biophysical basis of microscale droplets

The role of droplet morphology

The mechanical properties of biological tissues can be probed by directly observing the surface morphology of droplets. When a microscale droplet is injected into the interstitial spaces between cells, the surrounding tissue constrains the droplet, causing it to deviate from its equilibrium spherical shape under uniform pressure; the changes in

Table 1 | Biophysical forces across cellular and tissue scales

Mechanical loads	Typical sources, pathways and responses	Characteristic scales
Tension (pulling)	Cytoskeletal components and extracellular matrix–cell linkages on cell membranes[165]. Mechanochemical forces influence cell proliferation, differentiation, sorting and migration[166,167]	Force of 1–5 pN, approximately 11-nm step per myosin head upon muscle contraction[168], at focal adhesion around 30 nN (fibroblasts) to 70 nN (cardiomyocytes)[169,170]
Compression (pressing)	Embryonic morphogenic movements induce the expression of transcription factors and restore protein signalling pathways, which influence growth and differentiation[171,172]. Pressure-induced membrane tension enables osmotic regulation through mechanosensitive channels[173,174]	Expression of Twist in *Drosophila* stomodeal cells has been shown to be controlled by compressive forces as small as approximately 60 nN (ref. 171). Effective Young's modulus on the order of 50 MPa (ref. 175)
Shear (load tangential to a surface)	Fluid flow and cell movement generate tangential stresses on cell (extracellular) and organelle surfaces (intracellular). Fluid shear at the blood–vascular wall interface acts on endothelial cells, triggering biochemical cascades important for morphogenesis, homeostasis and pathogenesis in cardiovascular disease[176–178]	Approximately 10^{-2} to 10 Pa from blood flow in the human vascular system[179]
Bending (load that induces tension and compression on opposite faces)	Auditory signals have been hypothesized to be mediated by membrane-bending-induced flexoelectricity[72,85]. Acoustic stimuli are local deformations from a combination of tension and compression. At the cell surface, molecules unfold to mediate cell–cell and extracellular matrix–cell mechanosignalling[180,181]	The membrane's bending modulus k_b of lipid bilayers is small, around 10^{-21} to 10^{-19} J (ref. 175). Forces of 1–10 pN are required to unfold talin and integrin molecules on the cell surface[180,181]
Torsion (twisting)[a]	Motor proteins, including bacterial flagellar rotors and ATPases. Flagellar motors directly drive cellular movement, and torsion catalyses ATP synthesis at the active sites of F-type ATPase[182]	Measurements of torque generated by flagella can reach 4,000 pN nm^{-1}, and ATPases and other molecular systems generate torques of 5–40 pN nm^{-1} (ref. 182)

[a]The torsional mechanical loading is relatively underexplored regarding its effects at the cellular scale. Molecular-scale examples have been included for comparison.

droplet morphology depend on local mechanical forces and material properties.

The forces acting on the droplet surface include the hydrostatic pressure inside the droplet P_i; the hydrostatic pressure from the surrounding environment P_e; the local normal stress applied by the tissue at the droplet interface $\sigma_{nn}(\theta, \phi)$, specified by polar and azimuthal angles θ and ϕ, respectively; and the capillary force generated by surface tension γ along the interface that tends to restore a spherical shape (Fig. 1a). At each surface point, the capillary pressure follows the Young–Laplace equation $\Delta P = 2\gamma H(\theta, \phi)$, where $H(\theta, \phi)$ is the local mean curvature at the droplet interface[47]. Accordingly, the mechanical equilibrium at the droplet surface can be described as[48]:

$$P_i = P_e + 2\gamma H(\theta, \phi) - \sigma_{nn}(\theta, \phi) \quad (1)$$

To decouple the forces acting on the droplet, the tissue normal stress $\sigma_{nn}(\theta, \phi)$ is decomposed into two distinct components: an isotropic term σ_{nn}^{iso}, representing the average uniform compression, and an anisotropic term $\delta\sigma_{nn}(\theta, \phi)$, representing local deviatoric stresses. Therefore, $\sigma_{nn}(\theta, \phi) = \sigma_{nn}^{iso} + \delta\sigma_{nn}(\theta, \phi)$. Crucially, the isotropic tissue stress σ_{nn}^{iso} acts effectively as an addition to the external hydrostatic pressure and cannot be distinguished from P_e solely based on the droplet shape. To address this limitation, a reference spherical shape with radius R_{ref} is defined by fitting the droplet geometry. This reference sphere corresponds to the hypothetical equilibrium state under purely isotropic loads, in which $\delta\sigma_{nn}(\theta, \phi) = 0$. By definition[49], the mean curvature $H_{ref}(\theta, \phi)$ of a sphere is $\frac{1}{R_{ref}}$. Substituting these isotropic conditions into equation (1) yields the equilibrium expression for the reference state:

$$\Delta p = P_i - P_e + \sigma_{nn}^{iso} = 2\gamma H_{ref}(\theta, \phi) = \frac{2\gamma}{R_{ref}} \quad (2)$$

This equation demonstrates that the radius of the best-fit sphere, R_{ref}, is determined by the combined effect of the pressure difference and the mean isotropic stress. By subtracting the isotropic reference state (equation(2)) from the full equilibrium (equation(1)), the unknown hydrostatic and isotropic terms can be eliminated and the anisotropic term of the normal stress[50] can be obtained, which is exerted by the surrounding mechanical environment:

$$\delta\sigma_{nn}(\theta, \phi) = 2\gamma\left(H(\theta, \phi) - \frac{1}{R_{ref}}\right) \quad (3)$$

The surface curvature of a droplet embedded in tissue can be reconstructed using high-resolution imaging techniques, such as confocal microscopy, combined with computational image analysis[50]. Therefore, the measurement of the local curvature of the droplet can be used to quantify the anisotropic term of normal forces acting on the droplet from its surrounding environment.

Microscale droplets can contain mechanoresponsive materials, which can be used to perform externally actuated measurements of the dynamic mechanical properties of living tissues, such as local viscoelasticity. For instance, droplets made of ferrofluidic materials elongate under an applied magnetic field[34,51]. Such droplets can be injected into tissues and deformed by using externally controlled magnetic fields; imaging of the resulting morphological changes allows measurement of the viscoelastic properties of the surrounding tissue. The droplet deformation is set by the actuation force applied by the droplet, the restorative effect of the droplet surface tension and the viscoelastic resistance of the surrounding tissue[52] (Fig. 1a). Such deformation can be quantified by using a generalized Maxwell viscoelastic model. In this framework, the droplet–tissue interaction is represented by two Maxwell branches with elastic parameters (k_1, k_2) and viscous parameters (μ_1, μ_2), coupled in parallel with the droplet capillary stiffness $K_d = \frac{6\gamma}{R}$, where γ and R are the surface tension and initial radius of the droplet, respectively. The branch stiffness and viscosity parameters are related to the intrinsic elastic modulus E_i and viscosity η_i of the surrounding tissue through a

Box 1 | Definitions and relevant terminology of microscale droplets

In this rapidly evolving field, terminology is frequently debated, and classification criteria could be overlapping or misleading[183]. Our Review adopts a physics and bioengineering lens to examine the broader applications of microscale droplets. Here, we present a consistent set of definitions to support clarity throughout this Review.

Vesicles are droplets bounded by a continuous lipid or polymer bilayer membrane that separates a lumen from the external environment. Vesicles that are bound by lipids are termed liposomes, and those bound by polymers are termed polymersomes[21]. Microscale liposomes comparable with the size of cells are termed giant unilamellar vesicles, whereas analogous liposomes with internal bilayer structures are termed multilamellar vesicles[184]. Together, these are soft, microscale structures that serve as cell mimics in the study of biological mechanotransduction.

Colloidosomes are droplets encapsulated by a colloid shell, typically cross-linked. Colloidosomes encased by protein–polymer conjugates are termed proteinosomes[22,23]. These systems have been used to demonstrate cytoskeleton-free mechanotransduction, as evidenced by the mimicry of phagocytosis[118].

Coacervates are membraneless, polymer-rich droplets that can form through liquid–liquid phase separation of charged macromolecules[185]. They are useful in the assembly of artificial cytoskeletal networks important for mechanotransduction[117].

Emulsions are dispersions of bounded fluids, typically water and oil, stabilized by surfactants or lipids, but they are distinct from vesicles, as the phases are necessarily immiscible[24]. Emulsions have enabled in vivo mechanosensing of osmotic pressure in embryonic tissue[100].

Microgels are soft, hydrated polymer beads at the micrometre scale. Their porous nature enables dynamic swelling and shrinking, making them amenable to mechanoresponsive functions[99], and they have been used as stress sensors embedded in living tissue[99].

Droplet interface bilayers (DIBs) are bilayers that form at the interface between two monolayer-coated droplets[186], supporting mechanoelectrical processes such as mechanosensitive channel gating[69] and flexoelectricity[44], thereby acting as a fundamental component of intercommunicating droplet networks[39]. DIBs form when droplets are deposited into a surfactant-containing or lipid-containing oil, in which amphiphilic molecules rapidly self-assemble at the droplet surface to form a monolayer coating. When two such droplets are brought into contact in the oil phase, a metastable bilayer forms between them. DIBs can also be made from biological membranes harvested from cells[155]. Here, bilayer refers to a membrane formed by two opposing layers of amphiphilic molecules. In this Review, alternative bilayer-based droplet platforms, such as giant unilamellar vesicles, are also included within droplet-based systems but differ from DIBs in that their bilayer encloses a single compartment rather than forming at a droplet–droplet contact interface in oil.

Multisomes are multicompartment droplet assemblies in which multiple inner aqueous compartments are enclosed within a single outer oil phase, enabling transfer into aqueous or air environments while preserving internal bilayer connections[187].

Synthetic cells are engineered compartments that mimic selected properties of biological cells[25]. Synthetic tissues are patterned, communicating networks of synthetic cells that enable collective properties greater than the sum of their parts[39,134]. Hybrid tissues are synthetic tissues composed of both synthetic and living cells[188].

geometry-dependent scalar factor α, which is associated with the droplet deformation, such that $k_i = \alpha E_i$, $\mu_i = \alpha \eta_i$. Therefore, the effective elastic modulus E and viscosity η of the tissue are given by $E = E_1 + E_2$ and $\eta = \eta_1 + \eta_2$. When the droplet is deformed by a time-dependent magnetic stress $\sigma_{mag}(t)$, the evolution of its strain $\varepsilon(t)$ over time can be described by[34]

$$\varepsilon(t) = \sigma_{mag}(t)\left[\frac{1}{K_d} + A_1\left(1 - e^{-\frac{t}{\tau_1}}\right) + A_2\left(1 - e^{-\frac{t}{\tau_2}}\right)\right] \quad (4)$$

where $\tau_i = \frac{\mu_i}{k_i}$ are the relaxation timescales of the two Maxwell branches, and A_1 and A_2 are weighting coefficients determined from the viscoelastic parameters of the droplet materials. The time-dependent strain $\varepsilon(t)$ can be computed from the shape evolution of the droplet, typically estimated from the elliptical shape using the axis ratio $\varepsilon = \frac{2}{3}(\frac{b}{a} - 1)$, where b and a are the major and minor axes, respectively. By continuously monitoring $\varepsilon(t)$ through imaging and fitting to the above equation, the values of K_d, μ_i and k_i can be extracted, which can be used to calculate the elastic modulus E and viscosity η of the surrounding biological tissue. This approach has enabled the use of microscale droplets to probe the mechanics of living tissues in a dynamic manner. For example, in early zebrafish embryos and tailbud tissues, fluorescent oil droplets were microinjected into the tissue, and their time-dependent shape deformations were quantified in vivo to extract spatially resolved viscoelastic properties[34]. A more detailed discussion of this method is provided in the section 'Mechanosensitive droplets for in situ biomechanical probing'.

Surface-mediated mechanical measurement and mechanotransduction mechanisms

Mechanosensitive channels embedded in lipid membranes. One way to engineer mechanosensitive droplet systems is to incorporate mechanosensitive channels (MSCs) into lipid bilayers. MSCs are membrane proteins that respond to mechanical stimuli and convert mechanical forces into biochemical signals[53,54] (Fig. 1b). MSCs include the bacterial mechanosensitive channels of large conductance (MscL) and small conductance[55]; the vertebrate TWIK-related arachidonic acid-stimulated K^+ channel and TWIK-related K^+ channel (TREK)[56]; and eukaryotic mechanosensitive channels, such as Piezo1 and Piezo2 (refs. 57,58).

Two models could explain how force is transmitted to ion channels: the force-from-lipids (FFL) model and the force-from-tether (FFT) model[59]. In the FFL model, mechanical stimuli are transmitted directly through the lipid bilayer by membrane tension, thickness or curvature changes to activate the channel without the need for additional components such as the cytoskeleton or accessory proteins[59–62]. For example, MscL is considered inherently mechanosensitive and can be mechanically activated after purification and reconstitution into a lipid bilayer[33,55,63,64]. By contrast, the FFT model proposes that the pore-forming subunit is activated by forces transmitted through associated

extracellular matrix components or intracellular cytoskeletal elements such as actin filaments and microtubules, as exemplified by the channel no mechanoreceptor potential C (NOMPC)[65,66]. These two models are not mutually exclusive. Channels such as Piezo may integrate both FFL and FFT mechanisms produced by local changes in membrane tension and curvature, as well as forces transmitted through the cytoskeleton.

A common strategy to incorporate MSCs into lipid bilayers is detergent-assisted reconstitution[67], in which purified MSCs are solubilized in detergent, mixed with artificial lipid membranes and inserted into bilayers as the detergent is removed (through dialysis, for example). Another method is co-translational insertion using cell-free protein synthesis systems, in which MSC-encoding plasmids are combined with artificial membranes and cell extracts to enable MSC insertion during or after translation[67,68]. Once embedded, MSCs in droplets operate similarly to those in living cells: droplet deformation increases membrane tension, opening the channels and permitting ion transport. The resulting ion flux generates a transmembrane potential difference, which can be measured using patch-clamp techniques. The activation of MSCs can also initiate downstream chemical events, such as the translocation of a fluorescent dye and the activation of encapsulated reactions[44,69–71]. In this way, mechanical cues are transduced into electrical, optical or biochemical signals, providing a foundation for using MSCs incorporated into droplets to enable mechanical measurement and mechanotransduction.

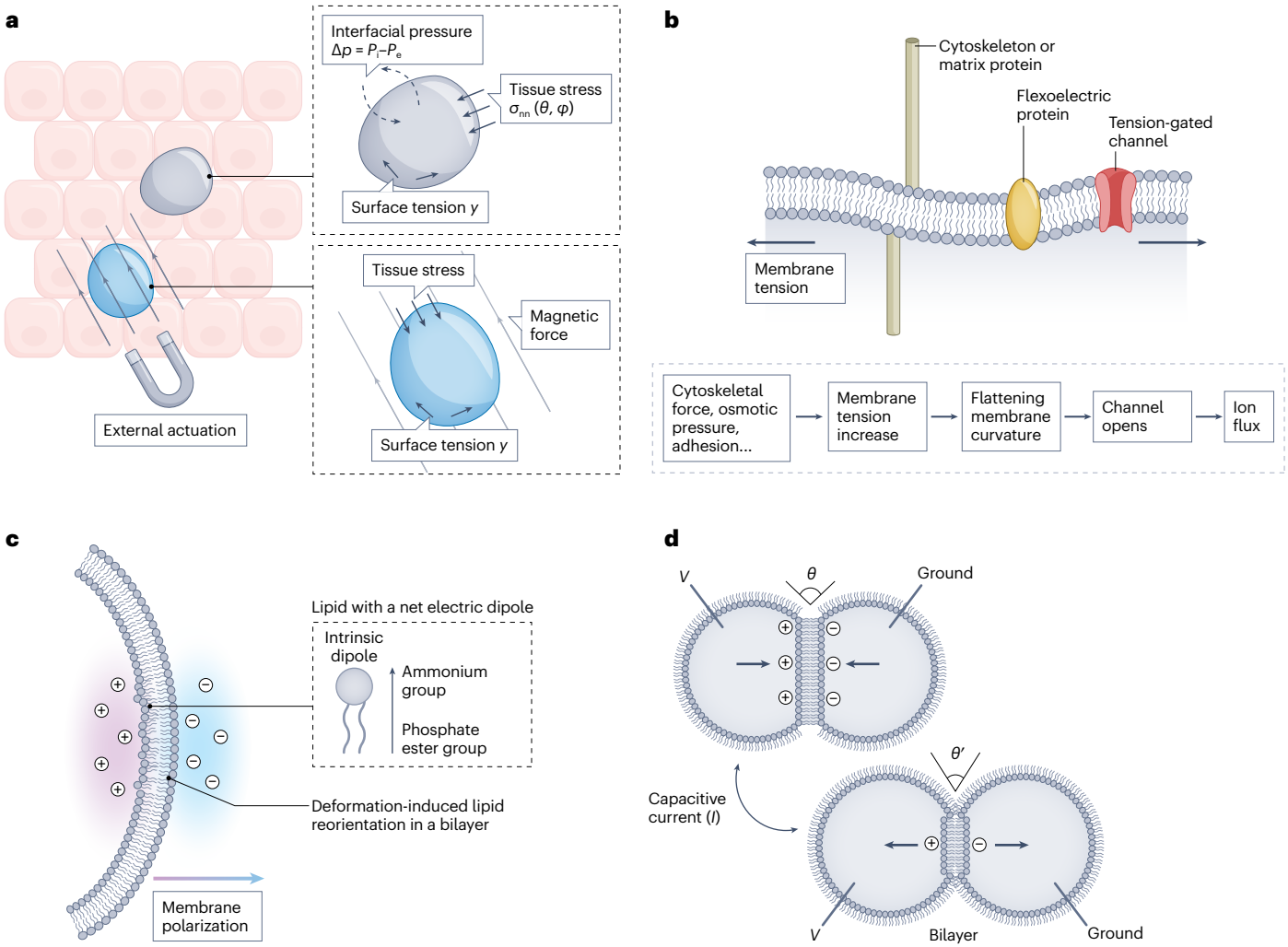

Fig. 1 | Biophysical mechanisms of droplet mechanical measurements and mechanotransduction. a, Droplet deformation under surrounding mechanical forces. At mechanical equilibrium, the droplet shape is determined by the balance between internal and external fluidic pressures (P_i and P_e, respectively), surface tension and local normal stress from the surrounding tissue (top). When droplet actuation is applied (for instance, a magnetic stimulus), droplet deformation is governed by a balance between the generated force, surface tension and reactive forces from the surrounding tissue (bottom). **b**, Mechanical stimuli can be transduced by membrane channels inserted in the lipid bilayer through membrane tension. Mechanical stimuli, including cytoskeletal forces, osmotic pressure and adhesion, can increase membrane tension and flatten membrane curvature, thereby opening tension-gated channels inserted in the lipid bilayer and enabling ion transport. **c**, Reorientation of dipolar lipids under curvature generates local flexoelectric polarization (cations and anions indicated by + and − signs, respectively). **d**, Mechanical compression and extension result in different DIB contact angles θ and θ' and change the capacitive current (I) under an applied voltage (V) through inserted electrodes.

Membrane flexoelectricity. The flexoelectric effect is a phenomenon in which an electrical polarization is induced by a mechanical strain gradient, allowing the direct coupling of an applied force and an electrical response[72]. Unlike the piezoelectric effect, in which electromechanical coupling occurs through a shift in charge distribution in solids belonging to non-centrosymmetric crystal point groups[73,74], the flexoelectric effect does not require such intrinsic asymmetry. Flexoelectric behaviours have been investigated in both solid-state structures[75,76] and soft materials[77,78] such as liquid crystals[72]. Owing to its ubiquity in soft, membrane-bound systems at the microscale, it has long been recognized as an important electromechanical mechanism for the study of both biochemical pathways and protocells[72,79].

For example, dipolar lipids can be analysed using the model of liquid crystal flexoelectricity. Because the lipids are cone shaped along their principal axis, flexoelectricity originates from the reorientation of lipids towards more energetically favourable alignments under curvature[77] (Fig. 1c). Under bending, one face of the lipid membrane experiences tensile strain, thereby pulling the material apart, whereas the opposite face undergoes compressive strain, thereby pushing the material inwards. This generates a strain gradient across the membrane, causing lipid reorientation and a net polarization along the radial axis of the curved deformation. The polarization generates a potential difference across the membrane, and a transient current can be measured as polarization changes over time[44,72], as described by the polarization current density:

$$\mathbf{J}_{\mathrm{p}} = \frac{\partial \mathbf{P}}{\partial t} \tag{5}$$

where $\mathbf{J}_{\mathrm{p}}$ is the induced current density, $\mathbf{P}$ is the polarization density and t is time. Experimental and theoretical studies of flexoelectricity in lipid bilayers showed that the magnitude of flexoelectric polarization is inversely proportional to the radius of curvature of the membrane R, with the proportionality constant f defined as the flexoelectric coefficient[79,80], such that

$$\mathbf{P} = -\frac{f}{R} \tag{6}$$

where the negative sign indicates that the polarization points towards the curvature centre. This relationship rationalizes the enhanced flexoelectric response in soft, microscale droplets, in which large curvature changes increase the strain gradient across a bilayer[81]. Moreover, because the curvature elastic modulus of lipid membranes is small, they can sustain a relatively large curvature strain in comparison to other load conditions, such as tensile or compressive strains[79].

In living systems, flexoelectricity and its converse, lipid reorientation in response to an electric potential[82,83], have been observed in diverse mechanosensitive and transduction processes. The examples of the involvement of biological flexoelectricity include bone remodelling[84] and auditory sensing[85,86], and flexoelectricity has even been hypothesized to mediate changes in the curvature of inner mitochondrial membranes when oxidative phosphorylation processes are active[79]. General models have been developed to describe many other mechanoelectrical systems in biology[87–89]. For example, in the inner ear, the membranes of stereocilia bundles in human hair cells generate electrical polarizations of up to 6 mV under patch-clamp recording when deflected by approximately 1 µm (ref. 85). In another example, patch-clamp studies of excised locust muscle membranes demonstrated that an oscillating pressure (345 Hz, 320 Pa peak) can elicit an alternating transmembrane current with a root mean square value of 9 pA[90]. This current has been hypothesized to arise from flexoelectric potentials that activate potassium BK and IK channels[90]. Interestingly, the converse flexoelectric effect can cause cell membrane twitching during an action potential[83].

Finally, droplet-based models[44], hair cell mimics[44,91] and soft energy-harvesting devices[92] inspired by these biophysical pathways have been experimentally studied. These studies suggest that the flexoelectric properties of lipid membranes can serve as a basis for mechanoresponsive droplet systems, providing a foundation for coupling these synthetic droplets with biological systems, enabled by their soft microscale nature[93]. Despite these fundamental proof-of-concept studies, there have been no examples of droplet devices that harness flexoelectricity or its converse effect for in vivo applications, suggesting much potential for future investigation.

Membrane capacitance. Another mechanical measurement approach for microscale droplets involves capacitive mechanotransduction. Bilayers are key mechanoresponsive units in biology, and DIBs, which are fundamental components of functional droplet networks[39], are a practical model system for the study of mechanoelectrical droplet interactions. A DIB can be modelled as a dielectric layer with a capacitance C proportional to its area A[94] (Fig. 1d). The compression of a droplet pair can dynamically alter the area of the DIB by altering the force balance at the triple-phase boundary (water–oil–water). Doing so changes its area, thereby modulating its capacitance, resulting in a capacitive current I_{cap} under an externally applied voltage V[44].

Importantly, although flexoelectric and capacitive effects are both active in lipid bilayer membranes, they operate through different mechanisms and produce different signals, possibly allowing parallel sensing. Flexoelectricity converts mechanical strain into electrical signals through a spontaneous polarization that depends on curvature. The capacitive current requires an external voltage and depends on changes in capacitance, primarily due to mechanically induced changes in the DIB surface area, with small contributions from changes in membrane thickness and the dielectric constant.

Under symmetric oscillations, the flexoelectric frequency aligns with the driving frequency, whereas the frequency of the capacitive current has been observed to be twice the driving frequency[44,95]. Theoretically, I_{cap} can be derived under constant membrane thickness, electric potential drop across the membrane φ and specific capacitance C_{s}. Differentiating the expression for the total charge of the capacitive membrane with variable A results in

$$I_{\mathrm{cap}} = \varphi\left(C_{\mathrm{s}}\frac{dA}{dt}\right) \tag{7}$$

By assuming the area of the spherical DIB is a quadratic function of the central displacement of the droplet bulge h, which depends on the droplet's elastic strain, we may incorporate the form of symmetrical oscillation $h = h_{\mathrm{var}}\sin(\omega t) + h_0$, where h_{var} is the amplitude of oscillation, ω is its angular frequency and h_0 is the initial displacement, to yield

$$I_{\mathrm{cap}} = 2\pi\omega\varphi C_{\mathrm{s}}\left(h_{\mathrm{var}}^2\sin(2\omega t) + h_0 h_{\mathrm{var}}\cos(\omega t)\right) \tag{8}$$

Inclusion of the flexoelectric terms within the same derivation allows the separation of capacitive and flexoelectric contributions to the total membrane current I_{mem} in terms of the flexoelectric coefficient f

$$I_{\mathrm{mem}} = 2\pi\omega[\varphi C_{\mathrm{s}}\left(h_{\mathrm{var}}^2\sin(2\omega t) + h_0 h_{\mathrm{var}}\cos(\omega t)\right) + 2hfh_{\mathrm{var}}\cos(\omega t)] \tag{9}$$

Hence, by measuring the capacitive current induced by DIB bulging, it may be possible to indirectly probe oscillatory forces in the cellular microenvironment. Such forces are important because they are hallmarks of dynamic biological processes, including oscillatory shear stresses acting on vascular endothelial cells, which have been implicated in the pathogenesis of atherosclerosis[96].

Implementation of microscale droplets

Mechanosensitive droplets for in situ biomechanical probing

Microscale droplets have emerged as powerful tools for measuring mechanical properties at intercellular and intracellular locations with high spatiotemporal resolution. Droplet systems generally operate in two modes: passive deformation (Fig. 2a), in which the static deformations of droplets map endogenous cell-generated forces, such as traction forces; and active probing, in which droplet-induced forces probe local mechanical properties, such as viscoelasticity.

Early studies of the passive mode used fluorocarbon oil droplets (4–80 µm in diameter) encapsulated in fluorescent phospholipid monolayer membranes[50]. When injected into the interstitial spaces of living tissues, these spherical microscale droplets deform due to cellular stresses. For example, measuring the local mean curvature $H(\theta, \phi)$ of a droplet surface through confocal 3D image stacks (Fig. 2b) enables measurement of the cellular stresses exerted by tooth mesenchymal cells in living mandible explants (Fig. 2c), thereby laying the foundation for studying force-mediated developmental processes[97].

However, the incompressibility of oil droplets limits their application to the measurement of isotropic normal stresses generated in living tissues, including between living cells[98]. To address this issue,

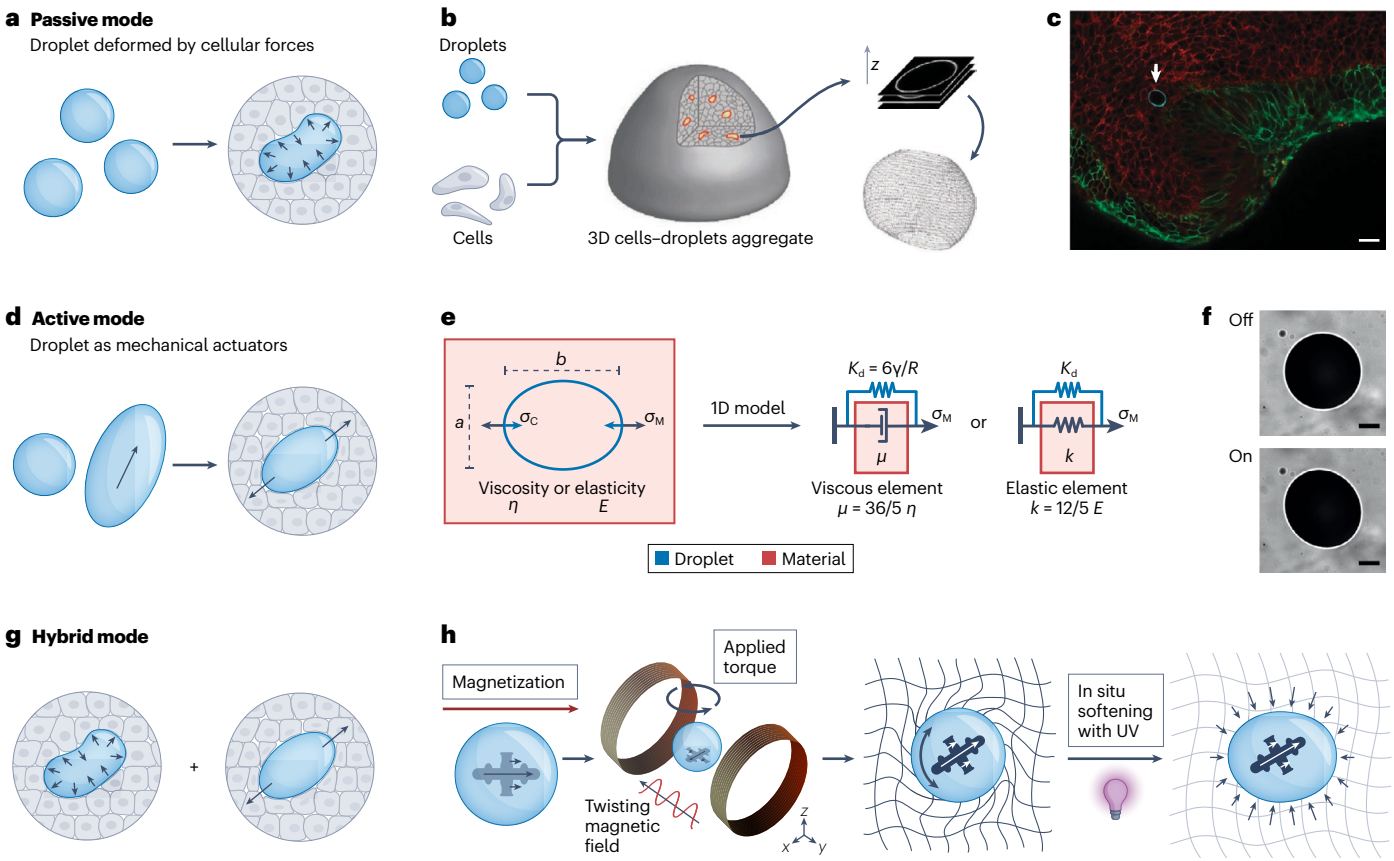

Fig. 2 | Mechanosensitive droplets for in situ mechanical probing. a, Droplet deformation by cellular forces and its function as a passive probe. **b**, Droplet sensors interface with living cells, enabling non-invasive, spatiotemporal and 3D sensing of mechanical forces in cell networks by fluorescence confocal microscopy. Functionalized droplets and cells are mixed to form aggregates. The droplet surface topology is then obtained by 3D confocal microscopy and image analysis. **c**, Droplet mechanosensor (cyan, arrow) located at the boundary between epithelial cells (green) and surrounding cells in developing mandible tissue (red). Scale bar, 20 µm. **d**, Droplets as mechanical actuators in the active mode. **e**, A ferrofluid droplet (blue) in a material (red) characterized by viscosity η or elasticity (stiffness) E. Magnetic stresses σ_M and capillary stress σ_C deform the ferrofluid droplet into an ellipsoid with major and minor axes b and a. Effective 1D diagrams representing the combined system of the droplet within a Newtonian fluid or elastic material, characterized by viscous μ and elastic k elements, respectively. K_d, droplet capillary stiffness. **f**, Fluorocarbon-based ferrofluid oil droplet in hydrocarbon oil, without ('off') and with ('on') magnetic field. Scale bars, 100 µm. **g**, The hybrid mode of a droplet-based mechanosensor. **h**, Using a droplet to measure stiffness and 3D traction forces. The droplet (blue) is permanently magnetized along the x axis (white arrow). A sinusoidal twisting magnetic field applied along the y axis generates an oscillatory magnetic torque about the z axis. The applied torque (grey arrow) deforms the surrounding microenvironment, enabling local stiffness measurements. Subsequently, the droplet probe is softened via 405-nm ultraviolet (UV) illumination, allowing the quantification of 3D traction forces exerted by surrounding cells on the droplet. Panels **b**, **c** adapted with permission from ref. 50, Springer Nature America, Inc. Panels **e**, **f** adapted with permission from ref. 34, Springer Nature America, Inc. Panel **h** adapted with permission from ref. 103, AAAS.

engineered polyacrylamide hydrogel droplets were developed as deformable stress sensors. Applications include injection of hydrogel droplets into 3D tumour spheroids to detect heterogeneous pressure distributions correlated with cell-shape anisotropy[98]. Despite the measurement capability of these droplets, the potential cytotoxicity of residual acrylamide monomers led to the development of more biocompatible alternatives. For example, elastic Arg-Gly-Asp-conjugated fluorescently labelled alginate microgels enable 3D displacement mapping and quantification of extracellular strain and traction forces[99]. These microgels have been validated in tumour-repopulating cell colonies and zebrafish embryos, demonstrating their capacity for dynamic stress quantification in living tissues.

Osmotic pressure is another key biomechanical regulator that can be detected by microscale droplets. Osmotic pressure sensors based on double-emulsion droplets (water-in-oil-in-water) have been developed[100], with an outer diameter of 20–80 µm. They contain fluorocarbon oils for the water-permeable oil phase and high-molecular-weight polyethylene glycol in the inner aqueous droplet to control its osmotic pressure. Changes in the osmolarity of the external medium drive water flow through the oil shell, causing changes in droplet shape and volume. Fluorescent dyes in both the inner droplet and the oil layer enable high-resolution quantification of inner and outer droplet sizes using confocal fluorescence microscopy. These sensors have been microinjected into zebrafish blastomeres and the interstitial spaces of developing embryonic tissues to measure extracellular osmotic pressure in vivo.

For the active mode (Fig. 2d), magnetically responsive ferrofluid oil droplets have been used to apply mechanical stresses on demand while simultaneously measuring tissue response[34]. Upon exposure to a uniform magnetic field, a droplet elongates along the field direction. As discussed *vide supra*, one can extract the dynamic mechanical properties of the local environment by tracking how the droplet deforms under sustained magnetic stress and recovers after its removal (Fig. 2e,f). Such magnetically responsive droplets (20–50 µm in diameter) have been injected to quantify the viscoelastic properties of zebrafish embryos during development. The size range is limited because capillary stresses dominate magnetic stresses as droplet size decreases, making droplets smaller than this range difficult to actuate and quantify. Larger droplets can also be generated, even up to hundreds of micrometres, but at the cost of invasiveness and reduced spatial resolution due to averaging over larger, mechanically heterogeneous regions.

Building on this technique, these active droplet probes have been used to investigate tissue plasticity. By embedding magnetically responsive droplets in zebrafish tissues and actively deforming them with an external magnetic field, it is possible to quantify the strain threshold marking the transition from reversible viscoelastic behaviour to irreversible plastic deformation. Such studies show that plasticity emerges when the applied deformation exceeds the cell–cell junction length, directly linking the onset of tissue plasticity to cell rearrangements within the foam-like cellular architecture[101].

However, ferrofluid droplets are constrained by low magnetic actuation forces, and stiffness values above 1 kPa are difficult to measure under typical experimental conditions[51]. This is because, as tissue stiffness increases, the induced strain progressively decreases, making the resulting shape changes difficult to quantify reliably using imaging. In addition, oil droplets may separate during tissue morphogenesis, limiting long-term monitoring. The requirement for specialized equipment, such as piezo stages, rotary motors and magnet arrays, further restricts broader applications[36].

To address these limitations, thermoresponsive microgels have been developed and injected into target tissues[36]. The microgels remain compacted at tissue culture temperatures (37 °C) but swell upon cooling below their lower critical solution temperature (approximately 34 °C). The degree of this expansion is constrained by the mechanical stiffness of the surrounding environment and can be quantified by imaging the gel dimensions. Such microgels have been dispersed into mouse tumour tissues. After tissue harvesting, the samples were immersed in a phosphate-buffered saline bath to control temperature conditions before the subsequent ex vivo measurement of tissue elasticity. This method makes it possible to probe local tissue elasticity at high spatial resolution. However, the inability to dynamically modulate temperature in vivo prevents real-time, in situ monitoring of disease progression.

More recently, fluorinated ferrofluid droplet systems have been advanced by extending the accessible timescale to approximately 1 hour and improving calibration strategies[35]. In mouse stem-cell-derived retinal organoids, magnetic droplets have been used to apply sustained stresses. Doing so enabled measurements over a broader time window, from seconds to tens of minutes, capturing mechanical responses relevant to organoid development. In addition, the applied magnetic stress was calibrated using viscous standards, thereby eliminating the need to directly measure the ferrofluid magnetization curve and simplifying experimental implementation. The resulting creep response is well described by a scale-free power-law rheology. The similar exponents reported in this case and in atomic force microscopy measurements of cells[102] suggest that the type of rheological behaviour may extend from the nanoscale to the microscale, a finding that links cell-scale mechanics to tissue-level dynamics.

Although these techniques have notably advanced the measurement of mechanical force distributions in tissues, a major challenge remains: the simultaneous, co-located quantification of 3D traction forces and stiffness (Fig. 2g). Traction force measurements require a soft, deformable probe, whereas quantification of stiffness necessitates a relatively rigid probe capable of exerting force. Achieving both properties simultaneously remains technically challenging. The challenges have been addressed by embedding biocompatible ferromagnetic cobalt-platinum microelements in Arg-Gly-Asp-conjugated stiff poly(ethylene glycol) droplets[103] (Fig. 2h). The droplets act as magnetically driven stiffness probes that rotate rigidly under an oscillatory magnetic field, which are used to report the local mechanical environment. Upon ultraviolet exposure, the poly(ethylene glycol) microgel degrades and softens, allowing the quantification of deformation and hence the measurement of 3D traction forces. These magneto-responsive droplets have been successfully applied to tumour-repopulating cell colonies and zebrafish embryos.

In addition, a photonic method based on whispering gallery modes has been developed to simultaneously measure local stiffness and internal anisotropic stress using droplet optical microcavities[104]. These droplets act as embedded mechanical sensors: upon deformation, spectral shifts in the whispering gallery modes occur—redshifts indicating expansion, and blueshifts indicating compression—enabling passive detection of anisotropic stress. To extract local stiffness, droplets are embedded in hydrogels and subjected to controlled external strains. Given the known droplet radius and the interfacial tension between the hydrogel and the droplet, the Young's modulus of the hydrogel is inferred from droplet aspect ratio changes (measured by spectral shifts) in response to a known applied strain. This dual-sensing strategy has been applied to ex vivo brain tissue. By monitoring spectral shifts,

the anisotropic stresses within the tissue can be quantified. However, this approach is limited to measurements of the equilibrium stiffness (Young's modulus) of biological materials under controlled ex vivo strain conditions; dynamic in vivo monitoring of biological tissues remains unexplored.

Droplet-based mechanotransduction for biotechnology

Droplets stand out for their ability to incorporate and compartmentalize biochemical components from the bottom-up[26,105]. A key goal is to endow droplets, often framed as synthetic cells or protocells, with the capacity for transduction—for example, converting mechanical inputs into biochemical, electrical or mechanical outputs, thereby converting force information into biosensing, drug delivery or soft microrobotic functions. Although these synthetic cell systems are at the proof-of-concept stage and do not yet have direct applications in living tissues, they provide manageable platforms for studying how compartmentalized microscale droplets can sense, encode and transduce mechanical cues, thereby revealing mechanotransduction principles to guide the engineering of droplet systems. For this reason, they are discussed here as simplified model systems that inform future applications in living cells and tissues.

We highlight three strategies that establish a chain from mechanical stimulus to functional actuation: reconstituting cytoskeletal machinery within droplets, harnessing interfacial physics for membrane remodelling and biomolecule transport, and integrating mechanosensitive proteins and synthetic gene circuits to couple sensing with signal processing and output.

In living cells, mechanotransduction is closely linked to the cytoskeleton, which is a dynamic network of actin and other filaments, motor proteins and associated regulators[106,107]. Cytoskeletal elements can be reconstituted within droplet systems in attempts to mimic the perception and responses of cells to mechanical cues[108,109] (Fig. 3a). For instance, purified actin networks have been introduced into microscale water-in-oil droplets with diameters of 4–30 μm (ref. 110) (Fig. 3b). Timelapse imaging revealed that actin filaments self-assembled into a single membrane-confined, ring-shaped bundle. In another example, actin filaments and myosin motors have been co-encapsulated within lipid vesicles, yielding synthetic compartments that undergo cell-like morphological transformations such as membrane blebbing, the formation of narrow membrane tubes (tethers) or the adoption of non-spherical, faceted morphologies[111].

In addition to actin-based systems, microtubule networks have also been successfully incorporated into giant unilamellar vesicles[109]. The microtubule networks within a droplet could be further engineered to respond to external magnetic or electric fields to facilitate internal cargo transport. Beyond native protein-based cytoskeletons, efforts have also been expanded to engineer artificial cytoskeletal networks using synthetic building blocks such as polymers[112], peptides[113], DNA[114,115] and small molecules[116]. An example of this approach involves amylose-based coacervates stabilized by a terpolymer membrane, in which a synthetic cytoskeleton is formed from polydiacetylene fibrils[117] (Fig. 3c). The fibrils self-assembled through electrostatic attraction between the negatively charged polydiacetylene filaments and the positively charged amylose-based coacervates, forming micrometre-sized cytoskeleton-like structures. These cytoskeletal mimics reduced the lateral movement (diffusivity) of the membrane component by up to sixfold relative to empty droplets and provided cell-like mechanical support with a Young's modulus of 0.4 ± 0.2 kPa, comparable with that of HL60 cells (0.5 ± 0.1 kPa). These results highlight the potential of integrating synthetic cytoskeletal elements to endow droplets with enhanced mechanical properties, advancing their use as functional biomimetic systems.

In addition to cytoskeletal reconstitution, purely artificial droplet systems can exploit interfacial properties to achieve mechanotransduction (Fig. 3d). One example emulates cellular processes such as endocytosis and exocytosis to enable targeted cargo loading and controlled release. In this approach, a water-in-oil magnetic Pickering emulsion (MPE) droplet was prepared using the spontaneous interfacial assembly of hydrophobic oleate-capped magnetite particles[118] (Fig. 3e). These MPE droplets, with an average diameter of 500 μm, were dispersed in a mixture of water and dodecane. The addition of oleic acid to the oil phase induced aperture formation in the MPE droplets, decreasing the oil–water interfacial tension. This change facilitated the spontaneous ingestion of water-filled silica colloidosomes by the MPE droplets, mimicking cell-like phagocytosis. Once internalized, the colloidosomes could subsequently release their payloads into the aqueous interior of the MPE, providing a platform for controlled delivery, multistage catalysis and complex bioassays involving sequential biochemical reactions.

Building on this concept, another system has been developed that enables bidirectional cross-membrane cargo transport driven by interfacial energy[119]. In this system, unilamellar liposomes undergo dynamic wetting and dewetting transitions in response to changes in interfacial tension, mimicking primitive cell-like behaviour. These changes in interfacial tension, controlled by environmental cues such as solvent evaporation, temperature shifts and osmotic pressure, enable the liposomes to internalize and transport biomolecules, including ions, DNA and enzyme substrates, providing a robust framework for advanced drug carriers.

A third strategy is to integrate mechanosensitive proteins and synthetic circuits to couple environmental sensing directly with adaptive responses (Fig. 3f). For example, inspired by the directional touch sensation of organisms, researchers have demonstrated that paired droplets containing reconstituted MscL can detect the direction of applied force[120]. This occurs because 'parallel' compression predominantly stretches the 1,2-diphytanoyl-*sn*-glycero-3-phosphocholine (DPhPC) monolayers while reducing the inter-droplet bilayer area, thereby increasing bilayer tension above the MscL gating threshold. By contrast, 'series' compression allows the bilayer to expand and relieves monolayer tension, producing insufficient bilayer tension for channel opening. Thus, distinct tension profiles generated by membrane geometry alone enable directional mechanotransduction.

Building on purely physical sensing, researchers have also incorporated gene circuits into droplets to enable mechanotransduction. One such system consitituted droplets containing an *Escherichia coli* cell-free transcription–translation system capable of sensing osmotic pressure and generating adaptive responses[121] (Fig. 3g). In these synthetic cells, the mechanosensitive channel MscL is reconstituted into the liposome bilayer membrane. When the external solution is made hypo-osmotic, membrane tension increases, the MscL opens and the otherwise membrane-impermeable inducer isopropyl-β-D-1-thiogalactopyranoside (IPTG) diffuses into the lumen. IPTG then activates the lac repressor and a LacO1/σ28-controlled transcription–translation system, driving the expression of a Venus–MreB fusion protein, in which the bacterial actin homologue MreB is fluorescently tagged and assembles into a coronal layer at the inner membrane. This architecture demonstrates how osmotic–mechanical cues can be converted into a programmable gene-expression output, providing a design blueprint

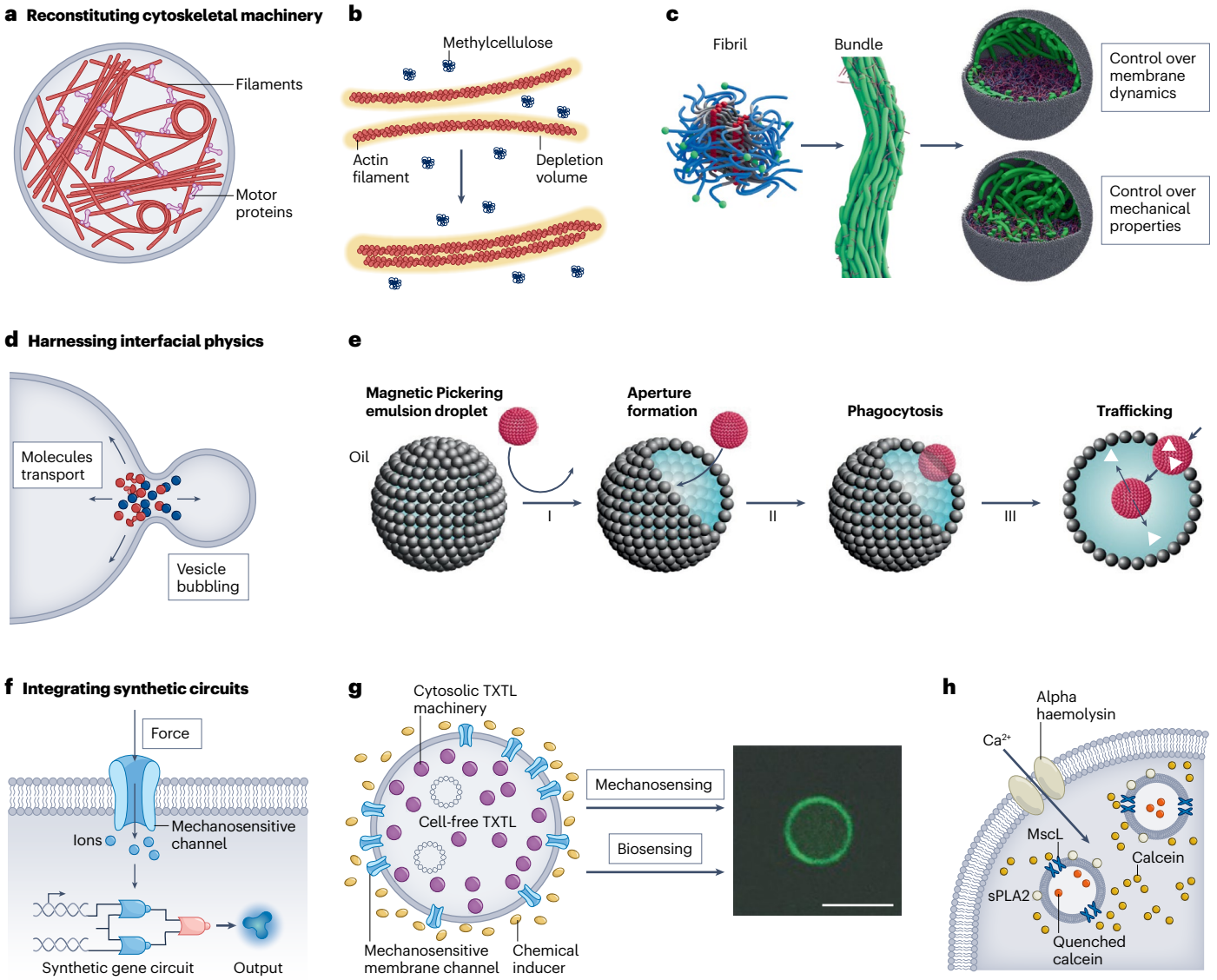

Fig. 3 | Droplet-based mechanotransduction for biotechnology. **a**, Reconstitution of cytoskeletal machinery within a droplet. **b**, The mechanism of actin bundling via the depletion effect. Macromolecules such as methylcellulose are excluded from the surface of actin filaments (yellow region). This depletion volume leads to an attractive force between actin filaments because a reduction in the depletion volume increases the entropy of the system, thereby lowering the total free energy. **c**, Incorporation of polydiacetylene fibrils into coacervates. **d**, The use of interfacial physics to drive membrane remodelling and transport in response to mechanical deformation. **e**, Spontaneous internalization of cross-linked, water-filled silica colloidosome (red) by larger water-in-oil magnetic Pickering emulsion droplets suspended in an oil continuous phase. Oleic acid induces aperture formation in the magnetic Pickering emulsion droplet, enabling artificial phagocytosis of the silica colloidosome. Encapsulated molecular payloads, represented by triangles, can then be trafficked and released on demand. **f**, Integration of a mechanosensitive protein and a synthetic gene circuit to couple mechanical sensing with signal processing and the functional output. **g**, Transition of a cell-free transcription–translation (TXTL) system from a quiescent to an active state, marked by the emergence of a cell-like cytoskeletal cortex in response to mechanical and chemical cues. Scale bar, 50 μm. **h**, A synthetic mechanosensitive signalling pathway based on calcium influx activates the secretory phospholipase A2 (sPLA2)–membrane–mechanosensitive channel of large conductance (MscL) cascade, resulting in content release and potential control of downstream events. Panel **b** adapted with permission from ref. 110, Springer Nature Ltd. Panel **c** adapted with permission from ref. 117, Springer Nature Ltd. Panel **e** adapted with permission from ref. 118, Springer Nature Ltd. Panel **g** adapted with permission from ref. 121, American Chemical Society. Panel **h** adapted with permission from ref. 122, National Academy of Sciences.

for responsive synthetic biosensors that sense mechanical stress and report it through user-defined biochemical responses.

Similarly, a synthetic mechanosensitive signalling pathway has been constructed within vesicle droplets by integrating phospholipase A_2 ($sPLA_2$) and MscLs[122] (Fig. 3h). Upon external calcium stimulation (uptake) through alpha haemolysin, $sPLA_2$ induces lipid asymmetry, thereby activating MscLs to release the incorporated cargo. This biomimetic signalling replicates key aspects of cellular

mechanotransduction, providing an environment-responsive molecular machine in biotechnology.

Outlook

Despite recent progress in the use of microdroplets for mechanical measurements and mechanotransduction, several challenges remain. First, current droplet mechanical sensors rely mostly on optical imaging to analyse droplet morphology. However, optical imaging of biological tissues is hindered by the scattering and absorption of light, which limit penetration depth[123,124]. As a result, these droplet sensors are restricted to superficial or otherwise optically accessible regions and cannot be applied in deep, multilayered or optically dense tissues[125]. This limitation impedes the broader application of droplet sensors for real-time monitoring in living organisms.

It is therefore essential to explore additional detection strategies that can enhance signal readout and enable wireless, implantable platforms for continuous in vivo monitoring of physiological signals. Ultrasound-based methods are promising. Previous studies have demonstrated the use of ultrasound for deep-tissue penetration and for quantifying stress in excised or in situ tumours[125], although spatial resolution has remained limited[26]. Conversely, advances in ultrasound technology are making wireless, implantable droplet-based sensors a more realistic prospect. For example, reports on in vivo 3D ultrasound imaging of organs using genetically encoded gas vesicles[126], ultrasound-mediated 3D printing in deep tissues[127] and long-term bioadhesive ultrasound imaging devices[128] have provided crucial conceptual and technical foundations for developing ultrasound-mediated droplet devices for in vivo monitoring. Nonetheless, scaling these capabilities down to the microscale or subcellular scale remains a major technical challenge.

Beyond ultrasound, intriguing research has focused on improving optical transparency in living animals[124]. One approach adds molecules with a high refractive index into the aqueous phase of tissues, reducing the refractive index mismatch between tissues and surrounding media, thereby enabling deeper and clearer tissue imaging[124]. This approach may open a new avenue for microscale droplet mechanosensors capable of real-time in vivo detection.

Another future direction is to use droplets as active tools to regulate tissue development. Increasing evidence suggests that the mechanical microenvironment within organoids or tissues, particularly interactions between cells and extracellular matrices, has a critical role in guiding cell differentiation and tissue morphogenesis[129–131]. This suggests the potential of droplet systems to function not only as passive sensors but also as active mechanical actuators capable of delivering targeted mechanical stimuli to influence development[132]. In particular, the converse flexoelectric effect may be harnessed to apply localized forces within soft, developing tissues such as organoids[133] or embryos[72].

A promising next step is the transition from individual droplets to DIB-based networks with more complex, coordinated functions[134–136]. Compared with isolated droplets, DIB-based networks provide well-defined droplet–droplet interfaces for testing whether mechanical perturbations propagate between compartments and whether such transmission is attenuated, amplified or blocked by network architecture[137]. This transition presents new opportunities for investigating tissue-level mechanotransduction[138–140].

Moreover, a DIB-based network can be arranged into spatially defined patterns to establish mechanical gradients. Such architectures may provide new matrix-like frameworks for modelling organoid development and, ultimately, for more precise mechanical regulation of tissue morphogenesis[45,46]. At a higher level of integration, droplet networks may combine mechanical sensing and actuation to achieve real-time, closed-loop control of the mechanical microenvironment[141]. Both biological nanopores and engineered nanofluidic channels, including synthetic polymer pores and DNA-based conduits[33,142,143], can insert into DIBs to mediate controlled signalling between droplets[144,145]. In addition, studies in model DIBs may be extended to alternative bilayer structures. For example, giant unilamellar vesicles are also amenable to membrane protein reconstitution[146] and to sensing stimuli such as salt concentration and temperature in aqueous conditions[147], while acting as promising cell mimics[148,149].

A key challenge in bringing such DIB-based droplet networks into physiological settings is that the DIBs are typically formed in oil phases that are not intrinsic to physiological environments[134]. Although buffer exchange can reduce bulk oil carryover and aid transfer into aqueous media, additional structural support is generally required to preserve network integrity. Strategies to provide such a supportive structure include the use of multisomes and hydrogel-based encapsulation. In multisomes, aqueous droplets are first assembled into a network and then encapsulated within a larger oil droplet dispersed in an external aqueous phase[150,151]. Another encapsulation-based strategy uses an agarose hydrogel as a supporting matrix, with lipid-containing oil compartments embedded within the matrix. After gelation, aqueous droplets are microinjected into these internal oil cavities to form lipid bilayers and generate communicating multicompartment structures[152]. More recently, jammed interconnected bilayer emulsions have been developed. Many bilayer-separated aqueous compartments are densely packed into a jammed droplet network, which shows mechanical stability in air and in aqueous environments[153].

Beyond physiological deployment, another challenge is that droplet networks differ substantially from structures with native biological membranes[154]. Simplified lipid composition and the lack of a cytoskeleton may alter membrane mechanics and force transmission, limiting the ability of the networks to recapitulate mechanotransduction in living tissues. Biomimetic designs, including the use of total lipid extracts, such as from *E. coli*[155], and the incorporation of asymmetric DIBs with independently defined leaflets[156], may help bridge the gap.

The spatial coordination of tissues also requires precise droplet positioning, a task that will be furthered by advances in 3D droplet printing[157]. Living cells can also be incorporated into droplets and printed into patterned networks[158]. For example, tissues derived from printed droplets with defined 3D geometries have been used to repair ex vivo brain tissue[158]. Moreover, 3D droplet printing holds promise for building physiologically relevant in vitro disease models with inherent 3D compartmentalization and heterogeneity—for example, to mimic the dynamic mechanical and biochemical changes that arise during tumour progression or fibrotic tissue remodelling[159]. Beyond precise positioning, magnetic guidance may provide additional opportunities for remote, on-demand dynamic regulation[160]. For instance, ferrofluids can be integrated into droplets, allowing magnetic fields to remotely manipulate droplet assemblies and dynamically separate and reform membrane interfaces[161].

Droplets are not limited to mimicking natural cell functions; they can also possess non-natural properties. For instance, droplets with tailored iontronic contents exhibit unique electrochemical behaviours[162–164], offering potential roles in tissue repair or as bioelectronic actuators such as synthetic pacemakers[42]. This ability to transcend biological constraints expands the functional repertoire of synthetic cells and tissues towards new modes of mechanobiological

intervention. We envision that the future of droplet-enabled mechanical measurements and mechanotransduction will drive advances in the understanding of the mechanical forces that shape life, while providing new tools to modulate the mechanobiological machinery for therapeutic purposes.

Published online: 14 September 2026

References

1. Mukherjee, P. et al. Role of mechanosensitive channels/receptors in atherosclerosis. *Am. J. Physiol. Cell Physiol.* **322**, C927–C938 (2022).
2. Aitken, C., Mehta, V., Schwartz, M. A. & Tzima, E. Mechanisms of endothelial flow sensing. *Nat. Cardiovasc. Res.* **2**, 517–529 (2023).
3. Hong, S. J. et al. Bio-inspired artificial mechanoreceptors with built-in synaptic functions for intelligent tactile skin. *Nat. Mater.* **24**, 1100–1108 (2025).
4. Brauer, A. M., Shi, H., Levin, P. A. & Huang, K. C. Physiological and regulatory convergence between osmotic and nutrient stress responses in microbes. *Curr. Opin. Cell Biol.* **81**, 102170 (2023).
5. Xu, H. et al. Bacterial–host adhesion dominated by collagen subtypes remodelled by osmotic pressure. *npj Biofilms Microbiomes* **10**, 124 (2024).
6. González-Martín, M., Martínez-Ara, G., Ngo, J. T., Trepat, X. & Roca-Cusachs, P. Synthetic mechanotransduction. *Nat. Rev. Bioeng.* **4**, 236–249 (2026).
7. Yang, S. et al. DNA-functionalized artificial mechanoreceptor for de novo force-responsive signaling. *Nat. Chem. Biol.* **20**, 1066–1077 (2024).
8. Stevens, A. J. et al. Programming multicellular assembly with synthetic cell adhesion molecules. *Nature* **614**, 144–152 (2023).
9. Kim, H. J., Chen, B., Suo, Z. & Hayward, R. C. Ionoelastomer junctions between polymer networks of fixed anions and cations. *Science* **367**, 773–776 (2020).
10. Dobashi, Y. et al. Piezoionic mechanoreceptors: force-induced current generation in hydrogels. *Science* **376**, 502–507 (2022).
11. Liu, M. et al. Robotic manipulation under harsh conditions using self-healing silk-based iontronics. *Adv. Sci.* **9**, 2102596 (2022).
12. Pan, H. & Lee, T. W. Recent progress in development of wearable pressure sensors derived from biological materials. *Adv. Healthc. Mater.* **10**, e2100460 (2021).
13. Liu, M., Tao, T. H. & Zhang, Y. Silk materials light up the green society. *Adv. Energy Sustainability Res.* **2**, 2100035 (2021).
14. Liu, M., Zhang, Y. & Tao, T. H. Recent progress in bio-integrated intelligent sensing system. *Adv. Intell. Syst.* **4**, 2100280 (2022).
15. Kim, G. et al. Ultrasound controlled mechanophore activation in hydrogels for cancer therapy. *Proc. Natl Acad. Sci. USA* **119**, e2109791119 (2022).
16. Vinikoor, T. et al. Injectable and biodegradable piezoelectric hydrogel for osteoarthritis treatment. *Nat. Commun.* **14**, 6257 (2023).
17. Donau, C. et al. Active coacervate droplets as a model for membraneless organelles and protocells. *Nat. Commun.* **11**, 5167 (2020).
18. Gao, N. & Mann, S. Membranized coacervate microdroplets: from versatile protocell models to cytomimetic materials. *Acc. Chem. Res.* **56**, 297–307 (2023).
19. Dewey, D. C., Strulson, C. A., Cacace, D. N., Bevilacqua, P. C. & Keating, C. D. Bioreactor droplets from liposome-stabilized all-aqueous emulsions. *Nat. Commun.* **5**, 4670 (2014).
20. Van de Cauter, L., van Buren, L., Koenderink, G. H. & Ganzinger, K. A. Exploring giant unilamellar vesicle production for artificial cells—current challenges and future directions. *Small Methods* **7**, 2300416 (2023).
21. Discher, D. E. & Eisenberg, A. Polymer vesicles. *Science* **297**, 967–973 (2002).
22. Li, R. Z., Liu, X. M. & Huang, X. Engineering proteinosomes with cellular-like functionalities. *ChemBioChem* **26**, e202500448 (2025).
23. Thompson, K. L., Williams, M. & Armes, S. P. Colloidosomes: synthesis, properties and applications. *J. Colloid Interface Sci.* **447**, 217–228 (2015).
24. Torre, P., Keating, C. D. & Mansy, S. S. Multiphase water-in-oil emulsion droplets for cell-free transcription–translation. *Langmuir* **30**, 5695–5699 (2014).
25. Spoelstra, W. K., Deshpande, S. & Dekker, C. Tailoring the appearance: what will synthetic cells look like? *Curr. Opin. Biotechnol.* **51**, 47–56 (2018).
26. Shang, L. & Zhao, Y. Droplet-templated synthetic cells. *Matter* **4**, 95–115 (2021).
27. Grashoff, C. et al. Measuring mechanical tension across vinculin reveals regulation of focal adhesion dynamics. *Nature* **466**, 263–266 (2010).
28. Blakely, B. L. et al. A DNA-based molecular probe for optically reporting cellular traction forces. *Nat. Methods* **11**, 1229–1232 (2014).
29. Chow, Y. T. et al. Single cell transfection through precise microinjection with quantitatively controlled injection volumes. *Sci. Rep.* **6**, 24127 (2016).
30. Aleksandrova, A., Rongish, B. J., Little, C. D. & Czirók, A. Active cell and ECM movements during development. *Methods Mol. Biol.* **1189**, 123–132 (2015).
31. Shakoor, A., Gao, W., Zhao, L., Jiang, Z. & Sun, D. Advanced tools and methods for single-cell surgery. *Microsyst. Nanoeng.* **8**, 47 (2022).
32. Mali, A. et al. Using tunable hydrogel microparticles to measure cellular forces. *Nat. Protoc.* **21**, 2301–2327 (2026).
33. Najem, J. S. et al. Activation of bacterial channel MscL in mechanically stimulated droplet interface bilayers. *Sci. Rep.* **5**, 13726 (2015).
34. Serwane, F. et al. In vivo quantification of spatially varying mechanical properties in developing tissues. *Nat. Methods* **14**, 181–186 (2017).
35. Shelton, E. R. et al. Scale invariance of mechanical properties in the developing mammalian retina. Preprint at *bioRxiv* https://doi.org/10.1101/2024.10.21.619491 (2025).
36. Mok, S. et al. Mapping cellular-scale internal mechanics in 3D tissues with thermally responsive hydrogel probes. *Nat. Commun.* **11**, 4757 (2020).
37. Holden, M. A., Needham, D. & Bayley, H. Functional bionetworks from nanoliter water droplets. *J. Am. Chem. Soc.* **129**, 8650–8655 (2007).
38. Villar, G., Graham, A. D. & Bayley, H. A tissue-like printed material. *Science* **340**, 48–52 (2013).
39. Booth, M. J., Restrepo Schild, V., Downs, F. G. & Bayley, H. Functional aqueous droplet networks. *Mol. Biosyst.* **13**, 1658–1691 (2017).
40. Zhang, Y. et al. A microscale soft ionic power source modulates neuronal network activity. *Nature* **620**, 1001–1006 (2023).
41. Liu, J. et al. Enzyme-enabled droplet biobattery for powering synthetic tissues. *Angew. Chem. Int. Ed.* **63**, e202408665 (2024).
42. Zhang, Y. et al. A microscale soft lithium-ion battery for tissue stimulation. *Nat. Chem. Eng.* **1**, 691–701 (2024).
43. Zhang, Y., Tan, C. M. J., Toepfer, C. N., Lu, X. & Bayley, H. Microscale droplet assembly enables biocompatible multifunctional modular iontronics. *Science* **386**, 1024–1030 (2024).
44. Freeman, E. C., Najem, J. S., Sukharev, S., Philen, M. K. & Leo, D. J. The mechanoelectrical response of droplet interface bilayer membranes. *Soft Matter* **12**, 3021–3031 (2016).
45. Gao, H. et al. Bio-orthogonal tuning of matrix properties during 3D cell culture to induce morphological and phenotypic changes. *Nat. Protoc.* **20**, 727–778 (2025).
46. Vega, S. L. et al. Combinatorial hydrogels with biochemical gradients for screening 3D cellular microenvironments. *Nat. Commun.* **9**, 614 (2018).
47. De Gennes, P.-G., Brochard-Wyart, F. & Quéré, D. *Capillarity and Wetting Phenomena: Drops, Bubbles, Pearls, Waves* (Springer Science & Business Media, 2003).
48. Boukellal, H., Campás, O., Joanny, J.-F., Prost, J. & Sykes, C. Soft *Listeria*: actin-based propulsion of liquid drops. *Phys. Rev. E* **69**, 061906 (2004).
49. Tapp, K. *Differential Geometry of Curves and Surfaces* Vol. 3 (Springer, 2016).
50. Campàs, O. et al. Quantifying cell-generated mechanical forces within living embryonic tissues. *Nat. Methods* **11**, 183–189 (2014).
51. Bijarchi, M. A., Favakeh, A., Sedighi, E. & Shafii, M. B. Ferrofluid droplet manipulation using an adjustable alternating magnetic field. *Sens. Actuators A* **301**, 111753 (2020).
52. Rowghanian, P., Meinhart, C. & Campàs, O. Dynamics of ferrofluid drop deformations under spatially uniform magnetic fields. *J. Fluid Mech.* **802**, 245–262 (2016).
53. Peyronnet, R., Tran, D., Girault, T. & Frachisse, J.-M. Mechanosensitive channels: feeling tension in a world under pressure. *Front. Plant. Sci.* **5**, 558 (2014).
54. Xiao, B. Mechanisms of mechanotransduction and physiological roles of PIEZO channels. *Nat. Rev. Mol. Cell Biol.* **25**, 886–903 (2024).
55. Perozo, E., Cortes, D. M., Sompornpisut, P., Kloda, A. & Martinac, B. Open channel structure of MscL and the gating mechanism of mechanosensitive channels. *Nature* **418**, 942–948 (2002).
56. Sorum, B., Docter, T., Panico, V., Rietmeijer, R. A. & Brohawn, S. G. Tension activation of mechanosensitive two-pore domain K^+ channels TRAAK, TREK-1, and TREK-2. *Nat. Commun.* **15**, 3142 (2024).
57. Beech, D. J. & Kalli, A. C. Force sensing by piezo channels in cardiovascular health and disease. *Arterioscler. Thromb. Vasc. Biol.* **39**, 2228–2239 (2019).
58. Syeda, R. Physiology and pathophysiology of mechanically activated PIEZO channels. *Annu. Rev. Neurosci.* **44**, 383–402 (2021).
59. Kefauver, J. M., Ward, A. B. & Patapoutian, A. Discoveries in structure and physiology of mechanically activated ion channels. *Nature* **587**, 567–576 (2020).
60. Martinac, B., Adler, J. & Kung, C. Mechanosensitive ion channels of *E. coli* activated by amphipaths. *Nature* **348**, 261–263 (1990).
61. Pliotas, C. et al. The role of lipids in mechanosensation. *Nat. Struct. Mol. Biol.* **22**, 991–998 (2015).
62. Kapsalis, C. et al. Allosteric activation of an ion channel triggered by modification of mechanosensitive nano-pockets. *Nat. Commun.* **10**, 4619 (2019).
63. Perozo, E., Kloda, A., Cortes, D. M. & Martinac, B. Physical principles underlying the transduction of bilayer deformation forces during mechanosensitive channel gating. *Nat. Struct. Biol.* **9**, 696–703 (2002).
64. Martinac, B. et al. Tuning ion channel mechanosensitivity by asymmetry of the transbilayer pressure profile. *Biophys. Rev.* **10**, 1377–1384 (2018).
65. Zhang, W. et al. Ankyrin repeats convey force to gate the NOMPC mechanotransduction channel. *Cell* **162**, 1391–1403 (2015).
66. Cox, C. D., Poole, K. & Martinac, B. Re-evaluating TRP channel mechanosensitivity. *Trends Biochem. Sci.* **49**, 693–702 (2024).
67. Boyd, M. A. & Kamat, N. P. Designing artificial cells towards a new generation of biosensors. *Trends Biotechnol.* **39**, 927–939 (2021).
68. Jacobs, M. L., Boyd, M. A. & Kamat, N. P. Diblock copolymers enhance folding of a mechanosensitive membrane protein during cell-free expression. *Proc. Natl Acad. Sci. USA* **116**, 4031–4036 (2019).
69. Barriga, H. M. G. et al. Droplet interface bilayer reconstitution and activity measurement of the mechanosensitive channel of large conductance from *Escherichia coli*. *J. R. Soc. Interface* **11**, 20140404 (2014).
70. Najem, J. S., Freeman, E. C., Yasmann, A., Sukharev, S. & Leo, D. J. Mechanics of droplet interface bilayer "unzipping" defines the bandwidth for the mechanotransduction response of reconstituted MscL. *Adv. Mater. Interfaces* **4**, 1600805 (2017).
71. Strutt, R. et al. Activating mechanosensitive channels embedded in droplet interface bilayers using membrane asymmetry. *Chem. Sci.* **12**, 2138–2145 (2021).

72. Nguyen, T. D., Mao, S., Yeh, Y.-W., Purohit, P. K. & McAlpine, M. C. Nanoscale flexoelectricity. *Adv. Mater.* **25**, 946–974 (2013).
73. Pohanka, M. The piezoelectric biosensors: principles and applications, a review. *Int. J. Electrochem. Sci.* **12**, 496–506 (2017).
74. Tressler, J. F., Alkoy, S. & Newnham, R. E. Piezoelectric sensors and sensor materials. *J. Electroceram.* **2**, 257–272 (1998).
75. Kołodziej, M. et al. Fundamentals of flexoelectricity, materials and emerging opportunities toward strain-driven nanocatalysts. *Small* **20**, 2406726 (2024).
76. Jia, L. et al. Flexoelectric effect in flexible 2D nanofluidic channels. *Faraday Discuss.* https://doi.org/10.1039/d5fd00134j (2026).
77. Petrov, A. G. Flexoelectricity of model and living membranes. *Biochim. Biophys. Acta* **1561**, 1–25 (2002).
78. Harland, B., Brownell, W. E., Spector, A. A. & Sun, S. X. Voltage-induced bending and electromechanical coupling in lipid bilayers. *Phys. Rev. E* **81**, 031907 (2010).
79. Petrov, A. G. Electricity and mechanics of biomembrane systems: flexoelectricity in living membranes. *Anal. Chim. Acta* **568**, 70–83 (2006).
80. Todorov, A. T., Petrov, A. G. & Fendler, J. H. First observation of the converse flexoelectric effect in bilayer lipid membranes. *J. Phys. Chem.* **98**, 3076–3079 (1994).
81. Todorov, A. T., Petrov, G., Brandt, M. & Fendler, J. H. Electrical and real-time stroboscopic interferometric measurements of bilayer lipid membrane flexoelectricity. *Langmuir* **7**, 3127–3137 (1991).
82. Zhang, P. C., Keleshian, A. M. & Sachs, F. Voltage-induced membrane movement. *Nature* **413**, 428–432 (2001).
83. Mosbacher, J., Langer, M., Hörber, J. K. H. & Sachs, F. Voltage-dependent membrane displacements measured by atomic force microscopy. *J. Gen. Physiol.* **111**, 65–74 (1998).
84. Vasquez-Sancho, F., Abdollahi, A., Damjanovic, D. & Catalan, G. Flexoelectricity in bones. *Adv. Mater.* **30**, 1705316 (2018).
85. Hudspeth, A. J. & Corey, D. P. Sensitivity, polarity, and conductance change in the response of vertebrate hair cells to controlled mechanical stimuli. *Proc. Natl Acad. Sci. USA* **74**, 2407–2411 (1977).
86. Breneman, K. D., Brownell, W. E. & Rabbitt, R. D. Hair cell bundles: flexoelectric motors of the inner ear. *PLoS ONE* **4**, e5201 (2009).
87. Petrov, A. G., Miller, B. A., Hristova, K. & Usherwood, P. N. R. Flexoelectric effects in model and native membranes containing ion channels. *Eur. Biophys. J.* **22**, 289–300 (1993).
88. Liu, L. P. & Sharma, P. Flexoelectricity and thermal fluctuations of lipid bilayer membranes: renormalization of flexoelectric, dielectric, and elastic properties. *Phys. Rev. E* **87**, 032715 (2013).
89. Galassi, V. V. & Wilke, N. On the coupling between mechanical properties and electrostatics in biological membranes. *Membranes* **11**, 478 (2021).
90. Petrov, A. G. Flexoelectricity and mechanotransduction. *Curr. Top. Membr.* **58**, 121–150 (2007).
91. Tamaddoni, N., Freeman, E. C. & Sarles, S. A. Sensitivity and directionality of lipid bilayer mechanotransduction studied using a revised, highly durable membrane-based hair cell sensor. *Smart Mater. Struct.* **24**, 065014 (2015).
92. Kancharala, A., Freeman, E. & Philen, M. A comprehensive flexoelectric model for droplet interface bilayers acting as sensors and energy harvesters. *Smart Mater. Struct.* **25**, 104007 (2016).
93. Mohammadkhah, M., Slavkovic, V. & Klinge, S. Flexoelectricity in biological materials and its potential applications in biomedical research. *Bioengineering* **12**, 579 (2025).
94. Gross, L. C. M., Heron, A. J., Baca, S. C. & Wallace, M. I. Determining membrane capacitance by dynamic control of droplet interface bilayer area. *Langmuir* **27**, 14335–14342 (2011).
95. Ochs, A. L. & Burton, R. M. Electrical response to vibration of a lipid bilayer membrane. *Biophys. J.* **14**, 473–489 (1974).
96. Himburg, H. A., Dowd, S. E. & Friedman, M. H. Frequency-dependent response of the vascular endothelium to pulsatile shear stress. *Am. J. Physiol. Heart Circ. Physiol.* **293**, H645–H653 (2007).
97. Mongera, A. et al. A fluid-to-solid jamming transition underlies vertebrate body axis elongation. *Nature* **561**, 401–405 (2018).
98. Dolega, M. E. et al. Cell-like pressure sensors reveal increase of mechanical stress towards the core of multicellular spheroids under compression. *Nat. Commun.* **8**, 14056 (2017).
99. Mohagheghian, E. et al. Quantifying compressive forces between living cell layers and within tissues using elastic round microgels. *Nat. Commun.* **9**, 1878 (2018).
100. Vian, A. et al. In situ quantification of osmotic pressure within living embryonic tissues. *Nat. Commun.* **14**, 7023 (2023).
101. Mongera, A. et al. Mechanics of the cellular microenvironment as probed by cells in vivo during zebrafish presomitic mesoderm differentiation. *Nat. Mater.* **22**, 135–143 (2023).
102. Hecht, F. M. et al. Imaging viscoelastic properties of live cells by AFM: power-law rheology on the nanoscale. *Soft Matter* **11**, 4584–4591 (2015).
103. Mohagheghian, E. et al. Quantifying stiffness and forces of tumor colonies and embryos using a magnetic microrobot. *Sci. Robot.* **8**, eadc9800 (2023).
104. Pirnat, G., Marinčič, M., Ravnik, M. & Humar, M. Quantifying local stiffness and forces in soft biological tissues using droplet optical microcavities. *Proc. Natl Acad. Sci. USA* **121**, e2314884121 (2024).
105. Ngocho, K. et al. Synthetic cells from droplet-based microfluidics for biosensing and biomedical applications. *Small* **20**, 2400086 (2024).
106. Fletcher, D. A. & Mullins, R. D. Cell mechanics and the cytoskeleton. *Nature* **463**, 485–492 (2010).
107. Brouhard, G. J. & Rice, L. M. Microtubule dynamics: an interplay of biochemistry and mechanics. *Nat. Rev. Mol. Cell Biol.* **19**, 451–463 (2018).
108. Ideses, Y. et al. Spontaneous buckling of contractile poroelastic actomyosin sheets. *Nat. Commun.* **9**, 2461 (2018).
109. Malik-Garbi, M. et al. Scaling behaviour in steady-state contracting actomyosin networks. *Nat. Phys.* **15**, 509–516 (2019).
110. Miyazaki, M., Chiba, M., Eguchi, H., Ohki, T. & Ishiwata, S. Cell-sized spherical confinement induces the spontaneous formation of contractile actomyosin rings in vitro. *Nat. Cell Biol.* **17**, 480–489 (2015).
111. Loiseau, E. et al. Shape remodeling and blebbing of active cytoskeletal vesicles. *Sci. Adv.* **2**, e1500465 (2016).
112. Chen, W., Kumari, J., Yuan, H., Yang, F. & Kouwer, P. H. J. Toward tissue-like material properties: inducing in situ adaptive behavior in fibrous hydrogels. *Adv. Mater.* **34**, e2202057 (2022).
113. Daly, M. L. et al. Designer peptide–DNA cytoskeletons regulate the function of synthetic cells. *Nat. Chem.* **16**, 1229–1239 (2024).
114. Zhan, P., Jahnke, K., Liu, N. & Göpfrich, K. Functional DNA-based cytoskeletons for synthetic cells. *Nat. Chem.* **14**, 958–963 (2022).
115. Arulkumaran, N., Singer, M., Howorka, S. & Burns, J. R. Creating complex protocells and prototissues using simple DNA building blocks. *Nat. Commun.* **14**, 1314 (2023).
116. Insua, I. & Montenegro, J. Synthetic supramolecular systems in life-like materials and protocell models. *Chem* **6**, 1652–1682 (2020).
117. Novosedlik, S. et al. Cytoskeleton-functionalized synthetic cells with life-like mechanical features and regulated membrane dynamicity. *Nat. Chem.* **17**, 356–364 (2025).
118. Rodríguez-Arco, L., Li, M. & Mann, S. Phagocytosis-inspired behaviour in synthetic protocell communities of compartmentalized colloidal objects. *Nat. Mater.* **16**, 857–863 (2017).
119. Tian, J.-Q. et al. Interfacial energy-mediated bulk transport across artificial cell membranes. *Nat. Chem. Eng.* **1**, 450–461 (2024).
120. Makhoul-Mansour, M. M. et al. A skin-inspired soft material with directional mechanosensation. *Bioinspir. Biomim.* **16**, 046014 (2021).
121. Garamella, J., Majumder, S., Liu, A. P. & Noireaux, V. An adaptive synthetic cell based on mechanosensing, biosensing, and inducible gene circuits. *ACS Synth. Biol.* **8**, 1913–1920 (2019).
122. Hindley, J. W. et al. Building a synthetic mechanosensitive signaling pathway in compartmentalized artificial cells. *Proc. Natl Acad. Sci. USA* **116**, 16711–16716 (2019).
123. Ntziachristos, V. Going deeper than microscopy: the optical imaging frontier in biology. *Nat. Methods* **7**, 603–614 (2010).
124. Ou, Z. et al. Achieving optical transparency in live animals with absorbing molecules. *Science* **385**, eadm6869 (2024).
125. Nia, H. T. et al. Solid stress and elastic energy as measures of tumour mechanopathology. *Nat. Biomed. Eng.* **1**, 0004 (2016).
126. Heiles, B. et al. Nonlinear sound-sheet microscopy: imaging opaque organs at the capillary and cellular scale. *Science* **388**, eads1325 (2025).
127. Davoodi, E. et al. Imaging-guided deep tissue in vivo sound printing. *Science* **388**, 616–623 (2025).
128. Wang, C. et al. Bioadhesive ultrasound for long-term continuous imaging of diverse organs. *Science* **377**, 517–523 (2022).
129. Huebsch, N. et al. Harnessing traction-mediated manipulation of the cell/matrix interface to control stem-cell fate. *Nat. Mater.* **9**, 518–526 (2010).
130. Hofer, M. & Lutolf, M. P. Engineering organoids. *Nat. Rev. Mater.* **6**, 402–420 (2021).
131. Panagaki, F. et al. Structural anisotropy results in mechano-directional transport of proteins across nuclear pores. *Nat. Phys.* **20**, 1180–1193 (2024).
132. Janmey, P. A. & Weitz, D. A. Dealing with mechanics: mechanisms of force transduction in cells. *Trends Biochem. Sci.* **29**, 364–370 (2004).
133. Jin, Y., Park, S. & Cho, S.-W. Organoid analytical toolkits. *Nat. Rev. Bioeng.* **4**, 336–352 (2026).
134. Villar, G., Heron, A. J. & Bayley, H. Formation of droplet networks that function in aqueous environments. *Nat. Nanotechnol.* **6**, 803–808 (2011).
135. Shang, L., Cheng, Y. & Zhao, Y. Emerging droplet microfluidics. *Chem. Rev.* **117**, 7964–8040 (2017).
136. Gobbo, P. et al. Programmed assembly of synthetic protocells into thermoresponsive prototissues. *Nat. Mater.* **17**, 1145–1153 (2018).
137. Rizzi, A. & Kim, S. Universal persistent Brownian motions in confluent tissues. *Phys. Rev. Lett.* **136**, 158401 (2026).
138. Souilhol, C. et al. Endothelial responses to shear stress in atherosclerosis: a novel role for developmental genes. *Nat. Rev. Cardiol.* **17**, 52–63 (2020).
139. Kurbel, S., Dodig, K. & Radic, R. The osmotic gradient in kidney medulla: a retold story. *Adv. Physiol. Educ.* **26**, 278–281 (2002).
140. Kim, M., Heo, G. & Kim, S.-Y. Neural signalling of gut mechanosensation in ingestive and digestive processes. *Nat. Rev. Neurosci.* **23**, 135–156 (2022).
141. Chong, Z. et al. Advances in networking droplets. *Droplet* **4**, e173 (2025).
142. Maraj, J. J. et al. Short-term facilitation-then-depression enables adaptive processing of sensory inputs by ion channels in biomolecular synapses. *ACS Appl. Electron. Mater.* **3**, 4448–4458 (2021).
143. Li, Z. et al. Ion transport and ultra-efficient osmotic power generation in boron nitride nanotube porins. *Sci. Adv.* **10**, eado8081 (2024).
144. Luo, J., Remy, A. & Zhang, Y. Iontronic devices from biological nanopores to artificial systems: emerging applications and future perspectives. *Chem. Rev.* **125**, 11840–11877 (2025).
145. Wang, L. et al. Neuromorphic iontronic devices based on soft ionic conductors. *Chem. Soc. Rev.* **55**, 299–335 (2026).

146. Jørgensen, I. L., Kemmer, G. C. & Pomorski, T. G. Membrane protein reconstitution into giant unilamellar vesicles: a review on current techniques. *Eur. Biophys. J.* **46**, 103–119 (2017).
147. Bolognesi, G. et al. Sculpting and fusing biomimetic vesicle networks using optical tweezers. *Nat. Commun.* **9**, 1882 (2018).
148. Litschel, T. & Schwille, P. Protein reconstitution inside giant unilamellar vesicles. *Annu. Rev. Biophys.* **50**, 525–548 (2021).
149. Wang, X., Du, H., Wang, Z., Mu, W. & Han, X. Versatile phospholipid assemblies for functional synthetic cells and artificial tissues. *Adv. Mater.* **33**, 2002635 (2021).
150. Cazimoglu, I., Booth, M. J. & Bayley, H. A lipid-based droplet processor for parallel chemical signals. *ACS Nano* **15**, 20214–20224 (2021).
151. Baxani, D. K. et al. Bilayer networks within a hydrogel shell: a robust chassis for artificial cells and a platform for membrane studies. *Angew. Chem. Int. Ed.* **55**, 14240–14245 (2016).
152. Bayoumi, M., Bayley, H., Maglia, G. & Sapra, K. T. Multi-compartment encapsulation of communicating droplets and droplet networks in hydrogel as a model for artificial cells. *Sci. Rep.* **7**, 45167 (2017).
153. Fica, A. et al. Jammed interconnected bilayer emulsions as 3D-printable biological tissue mimics. *Nat. Mater.* **25**, 1623–1633 (2026).
154. Chao, Y. & Shum, H. C. Emerging aqueous two-phase systems: from fundamentals of interfaces to biomedical applications. *Chem. Soc. Rev.* **49**, 114–142 (2020).
155. Taylor, G. J. & Sarles, S. A. Heating-enabled formation of droplet interface bilayers using *Escherichia coli* total lipid extract. *Langmuir* **31**, 325–337 (2015).
156. Hwang, W. L., Chen, M., Cronin, B., Holden, M. A. & Bayley, H. Asymmetric droplet interface bilayers. *J. Am. Chem. Soc.* **130**, 5878–5879 (2008).
157. Bachler, S., Haidas, D., Ort, M., Duncombe, T. A. & Dittrich, P. S. Microfluidic platform enables tailored translocation and reaction cascades in nanoliter droplet networks. *Commun. Biol.* **3**, 769 (2020).
158. Jin, Y. et al. Integration of 3D-printed cerebral cortical tissue into an ex vivo lesioned brain slice. *Nat. Commun.* **14**, 5986 (2023).
159. Chin, L., Xia, Y., Discher, D. E. & Janmey, P. A. Mechanotransduction in cancer. *Curr. Opin. Chem. Eng.* **11**, 77–84 (2016).
160. Wauer, T. et al. Construction and manipulation of functional three-dimensional droplet networks. *ACS Nano* **8**, 771–779 (2014).
161. Makhoul-Mansour, M. M., El-Beyrouthy, J. B., Mao, L. & Freeman, E. C. Enhancing membrane-based soft materials with magnetic reconfiguration events. *Sci. Rep.* **12**, 1703 (2022).
162. Lyu, Y., Su, Y., Nan, K. & Zhang, Y. Bioinspiration for biointronics. *Iontronics* **2**, 9 (2026).
163. Zhang, Y. & Bayley, H. Signals through salt: building machines that use the language of biology. *Phys. Today* **79**, 60–62 (2026).
164. Zhang, Y. & Bayley, H. Bioiontronics. *Nat. Rev. Bioeng.* https://doi.org/10.1038/s44222-026-00471-1 (2026).
165. Discher, D. E., Janmey, P. & Wang, Y.-l Tissue cells feel and respond to the stiffness of their substrate. *Science* **310**, 1139–1143 (2005).
166. Chen, C. S. Mechanotransduction—a field pulling together? *J. Cell Sci.* **121**, 3285–3292 (2008).
167. Parsons, J. T., Horwitz, A. R. & Schwartz, M. A. Cell adhesion: integrating cytoskeletal dynamics and cellular tension. *Nat. Rev. Mol. Cell Biol.* **11**, 633–643 (2010).
168. Finer, J. T., Simmons, R. M. & Spudich, J. A. Single myosin molecule mechanics: piconewton forces and nanometre steps. *Nature* **368**, 113–119 (1994).
169. Balaban, N. Q. et al. Force and focal adhesion assembly: a close relationship studied using elastic micropatterned substrates. *Nat. Cell Biol.* **3**, 466–472 (2001).
170. Tan, J. L. et al. Cells lying on a bed of microneedles: an approach to isolate mechanical force. *Proc. Natl Acad. Sci. USA* **100**, 1484–1489 (2003).
171. Desprat, N., Supatto, W., Pouille, P.-A., Beaurepaire, E. & Farge, E. Tissue deformation modulates twist expression to determine anterior midgut differentiation in *Drosophila* embryos. *Dev. Cell* **15**, 470–477 (2008).
172. Zhang, H. et al. A tension-induced mechanotransduction pathway promotes epithelial morphogenesis. *Nature* **471**, 99–103 (2011).
173. Sukharev, S. I., Blount, P., Martinac, B., Blattner, F. R. & Kung, C. A large-conductance mechanosensitive channel in *E. coli* encoded by mscL alone. *Nature* **368**, 265–268 (1994).
174. Martinac, B., Buechner, M., Delcour, A. H., Adler, J. & Kung, C. Pressure-sensitive ion channel in *Escherichia coli*. *Proc. Natl Acad. Sci. USA* **84**, 2297–2301 (1987).
175. Israelachvili, J. N. *Intermolecular and Surface Forces* (Academic Press, 2010).
176. Davies, P. F. Flow-mediated endothelial mechanotransduction. *Physiol. Rev.* **75**, 519–560 (1995).
177. Guillot, C. & Lecuit, T. Mechanics of epithelial tissue homeostasis and morphogenesis. *Science* **340**, 1185–1189 (2013).
178. Chien, S. Mechanotransduction and endothelial cell homeostasis: the wisdom of the cell. *Am. J. Physiol. Heart Circ. Physiol.* **292**, H1209–H1224 (2007).
179. Cheng, C. K., Wang, N., Wang, L. & Huang, Y. Biophysical and biochemical roles of shear stress on endothelium: a revisit and new insights. *Circ. Res.* **136**, 752–772 (2025).
180. Yao, M. et al. The mechanical response of talin. *Nat. Commun.* **7**, 11966 (2016).
181. Chen, Y., Lee, H., Tong, H., Schwartz, M. & Zhu, C. Force regulated conformational change of integrin αVβ3. *Matrix Biol.* **60-61**, 70–85 (2017).
182. Forth, S., Sheinin, M. Y., Inman, J. & Wang, M. D. Torque measurement at the single-molecule level. *Annu. Rev. Biophys.* **42**, 583–604 (2013).
183. Adamala, K. P. et al. Present and future of synthetic cell development. *Nat. Rev. Mol. Cell Biol.* **25**, 162–167 (2024).
184. Fletcher, M., Elani, Y., Keyser, U. F. & Tivony, R. Giant unilamellar vesicles as a model system for studying ion transport. *Biophys. Rev.* **17**, 1105–1118 (2025).
185. Lin, Z., Beneyton, T., Baret, J.-C. & Martin, N. Coacervate droplets for synthetic cells. *Small Methods* **7**, 2300496 (2023).
186. Bayley, H. et al. Droplet interface bilayers. *Mol. Biosyst.* **4**, 1191–1208 (2008).
187. Dimitriou, P. et al. Manipulation of encapsulated artificial phospholipid membranes using sub-micellar lysolipid concentrations. *Commun. Chem.* **7**, 120 (2024).
188. Bayley, H., Cazimoglu, I. & Hoskin, C. E. G. Synthetic tissues. *Emerg. Top. Life Sci.* **3**, 615–622 (2019).

Acknowledgements

This work was supported by the École Polytechnique Fédérale de Lausanne (to Y.Z.), the Novartis Foundation for Medical-Biological Research (25C081 to Y.Z.) and the Swiss National Science Foundation (10005601 to Y.Z.).

Author contributions

Y.S., N.S. and Y.Z. conceived the idea. All authors participated in writing and revising the manuscript.

Competing interests

The authors declare no competing interests.

Additional information

Peer review information *Nature Reviews Physics* thanks Friedhelm Serwane and the other, anonymous, reviewer(s) for their contribution to the peer review of this work.